Autler-Townes splitting via frequency up-conversion at ultralow-power levels in cold ^{87}Rb atoms using an optical nanofiber

Ravi Kumar,[1,2] Vandna Gokhroo,[1] Kieran Deasy,[1] and Síle Nic Chormaic[1,*]

[1]*Light-Matter Interactions Unit, Okinawa Institute of Science and Technology Graduate University, Onna, Okinawa 904-0495, Japan*

[2]*Physics Department, University College Cork, Cork, Ireland*

(Received 12 February 2015; published 22 May 2015)

The tight confinement of the evanescent light field around the waist of an optical nanofiber makes it a suitable tool for studying nonlinear optics in atomic media. Here, we use an optical nanofiber embedded in a cloud of laser-cooled ^{87}Rb for near-infrared frequency up-conversion via a resonant two-photon process. Sub-nW powers of the two-photon radiation, at 780 and 776 nm, copropagate through the optical nanofiber and the generation of 420 nm photons is observed. A measurement of the Autler-Townes splitting provides a direct measurement of the Rabi frequency of the 780 nm transition. Through this method, dephasings of the system can be studied. In this work, the optical nanofiber is used as an excitation and detection tool simultaneously, and it highlights some of the advantages of using fully fibered systems for nonlinear optics with atoms.

DOI: 10.1103/PhysRevA.91.053842 PACS number(s): 42.81.−i, 42.65.−k, 32.10.−f, 42.50.Hz

I. INTRODUCTION

Subwavelength diameter optical fibers, also known as optical nanofibers (ONFs), have recently emerged as a very useful tool for probing [1–3] and trapping cold atoms [4,5], particularly due to the functionality of such nanofibers in the development of atom-photon hybrid quantum systems [6,7]. Aside from this research focus, ONFs have also been shown to be highly efficient tools for demonstrating nonlinear optics using very-low-light power levels in atomic systems [8]. More than a decade ago, Patnaik *et al.* [9] proposed a demonstration of slow light in an ONF surrounded by a nonlinear medium, such as atoms. More recently, two-photon absorption by laser-cooled atoms using an ONF was proposed [10]. Quantum interference effects, such as electromagnetically induced transparency (EIT) [11] and two-photon absorption [12], were demonstrated using an ONF in rubidium (Rb) vapor, and nW-level saturated absorption in a Xe gas was observed with an ONF [13]. This versatility of ONFs for nonlinear optics arises from the very high evanescent field intensities that can be achieved as a result of the very tight light confinement within a very small mode area over long distances of a few mm, and it is known that atoms experience an appreciable ac Stark shift on their energy levels in the presence of an intense light field. Here, we study a two-photon excitation process, at 780 and 776 nm, in a cascade three-level configuration [14] in cold ^{87}Rb atoms using an optical nanofiber. We have observed frequency up-conversion for 776 nm probe power as low as 200 pW and Autler-Townes (A-T) splitting [15] for $<$20 nW of 780 nm coupling power. These power levels are several orders of magnitude lower than those used in free-space experiments [16–18]. The effect of varying the coupling power on the obtained A-T spectra is investigated and sources of dephasing within the system are considered.

*sile.nicchormaic@oist.jp

II. EXPERIMENTAL DETAILS

We use laser-cooled ^{87}Rb atoms, in a standard magneto-optical trap (MOT) configuration, the details of which are described elsewhere [19]. We adopt a two-photon cascade system where $5S_{1/2}$ ($|1\rangle$) is the ground state, $5P_{3/2}$ ($|2\rangle$) is the intermediate state, and $5D_{5/2}$ ($|3\rangle$) is the excited state. Relaxation of $|3\rangle$ via $6P_{3/2}$ ($|4\rangle$) generates 420 nm blue light (Fig. 1). A schematic of the experimental setup is shown in Fig. 2. A Rb vapor cell is used to provide the reference frequencies for the two-photon transitions. A counterpropagating configuration is chosen since the linewidths are solely determined by the lifetime of the final state in this configuration, $|3\rangle$ [20], and sharper peaks can be observed for reference purposes. The 420 nm blue fluorescence (ω_4) generated in the vapor cell is monitored using a photomultiplier tube (PMT) with the aperture covered by a 420 nm filter (FWHM of 10 nm). We do not detect the infrared 5.23 μm (ω_3) photons. All lasers used are extended cavity diode lasers (ECDLs), one of which is locked to the $5S_{1/2}\ F = 2 \rightarrow 5P_{3/2}\ F' = 2$ and $F' = 3$ crossover transition using a standard saturation absorption setup. This laser provides both the cooling beams for the MOT and the 780 nm coupling beam for the $|1\rangle \rightarrow |2\rangle$ transition (i.e., the $5S_{1/2}\ F = 2 \rightarrow 5P_{3/2}\ F' = 3$ transition). The second ECDL, at 776 nm, is scanned across the $|2\rangle \rightarrow |3\rangle$ probe transitions. A third ECDL (not shown in Fig. 2) is used for the 780 nm repump beam in the MOT.

The ONF is prepared from a commercial single-mode optical fiber for 780 nm using a flame brushing technique [21]. It has a diameter of $\sim$350 nm, ensuring that only the fundamental mode propagates at 780 nm. Note that higher modes may propagate in the ONF for 420 nm light. Transmission through the ONF at 780 nm is measured to be 84%. The ONF is mounted on an aluminium U-shaped mount and installed vertically in the vacuum chamber [2]. The experiment is designed so that the cold-atom cloud is centered on the waist of the ONF. The atom-cloud diameter is $\sim$0.8 mm and the temperature is measured to be $\sim$200 μK using a time-of-flight technique. The cloud position is optimized using two magnetic shim coils in order to overlap the densest part of the cloud to the ONF. This is done while monitoring the spontaneous emission from the atoms coupling into the ONF. The cloud

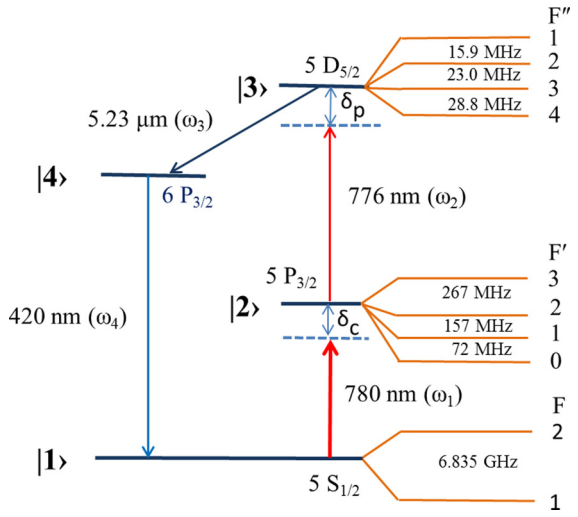

FIG. 1. (Color online) Energy-level diagram for ^{87}Rb atoms showing the 780 nm coupling and 776 nm probe beams.

contains $\sim 10^7$ atoms; however, if we consider the evanescent field decay length for 780 nm light, there are typically <10 atoms in the evanescent field region, and the photon signals collected via the ONF can be considered to be directly related to emissions from such low atom numbers.

The 780 and 776 nm beams used in the vapor cell reference measurements (ω_1' and ω_2', respectively) are split in order to obtain the required frequencies (ω_1 and ω_2, respectively) for two-photon excitation in the cold atoms via the ONF. The 780 nm beam from the ECDL is double passed through the acousto-optic modulator AOM2 (Fig. 2) using the "+1" order to obtain ω_1, which is 14 MHz red detuned from the $5S_{1/2}$ $F = 2$ to $5P_{3/2}$ $F' = 3$ cooling transition. The 776 nm beam from the second ECDL is double passed through AOM3 using the

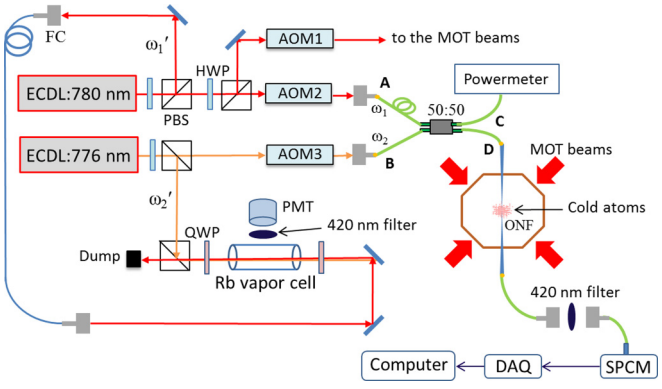

FIG. 2. (Color online) Schematic of the experimental setup. 780 and 776 nm light are copropagating in the nanofiber to generate blue photons from the cold atoms. An SPCM is used to detect the blue photons exiting from the nanofiber pigtail after filtering in free space. 780 and 776 nm light counterpropagating in a Rb vapor cell are used to obtain the reference signal for identification of the peaks in the two-photon spectrum. SPCM: single-photon counting module; ECDL: extended cavity diode laser; AOM: acousto-optic modulator; QWP: quarter waveplate; HWP: half waveplate; PMT: photomultiplier tube; MOT: magneto-optical trap; ONF: optical nanofiber; DAQ: data-acquisition card; FC: fiber coupler.

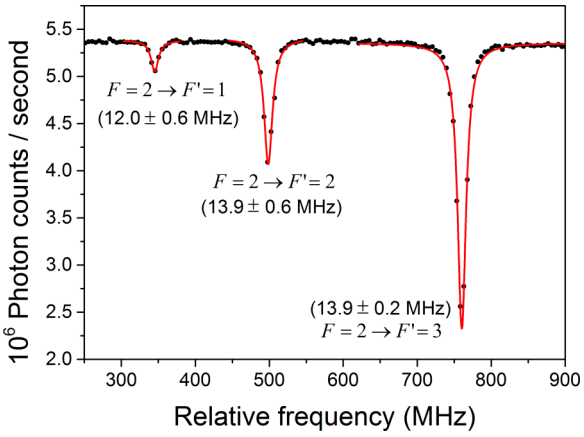

FIG. 3. (Color online) Transmission of 780 nm light passing through the ONF with cold ^{87}Rb atoms around the waist. The laser is scanning across the $5S_{1/2}$ $F = 2$ to $5P_{3/2}$ possible transitions. This spectrum is obtained using an additional ECDL laser in scan mode. The data are fit (red curves) to Lorentzian profiles and the obtained linewidths for the relevant transitions are indicated at the peaks.

"-1" order to ensure that $\omega_1' + \omega_2' = \omega_1 + \omega_2$. This permits us to directly compare the spectra obtained from the cold atoms and the vapor cell in real time. Circular polarization of the same handedness is used for all 780 and 776 nm excitation beams.

ω_1 is sent through port A of a 50:50 fiber beam splitter, while ω_2 passes through port B (Fig. 2). In order to excite the cold ^{87}Rb atoms from $|1\rangle$ to $|3\rangle$ in the two-photon cascade system via the ONF, one output port, D, of the fiber splitter is spliced to one pigtail of the nanofiber (Fig. 2). The other output port, C, is connected to a power meter to monitor beam powers. The measured power is proportional to the power at the nanofiber waist, with any differences arising from the ONF transmission losses at a particular wavelength. Hence, if we assume equal losses on both sides of the taper, the measured power can be taken as 1.1 times the waist power for both 780 and 776 nm wavelengths.

III. RESULTS AND DISCUSSIONS

A typical transmission spectrum of the 780 nm light (for input power of 1.8 nW) through the ONF is shown in Fig. 3 with no ω_2 present. As the laser is scanned across the $5S_{1/2}$ $F = 2$ to $5P_{3/2}$ F' transitions, absorption dips appear. If we add ω_2 into the nanofiber, 420 nm (blue) photons are generated within the atom cloud via four-wave mixing for copropagating coupling and probe beams [22]. ω_1 and ω_2 excite the atoms from $|1\rangle$ to $|3\rangle$ via $|2\rangle$. In the relaxation process from $|3\rangle$ to $|4\rangle$ and from $|4\rangle$ to $|1\rangle$, ω_3 ($\vec{k}_{IR}$) and ω_4 ($\vec{k}_{\text{blue}}$) are generated, respectively. The decay probability from $|3\rangle$ to $|4\rangle$ is 35% and from $|4\rangle$ to $|1\rangle$ is 31% [23]. The four frequencies are related by the frequency-matching condition to satisfy conservation of energy, $\omega_1 + \omega_2 = \omega_3 + \omega_4$, whereas momentum conservation requires the phase-matching relation $\vec{k}_{780} + \vec{k}_{776} = \vec{k}_{IR} + \vec{k}_{\text{blue}}$ to be satisfied [24]. In this system, the phase-matching condition must be satisfied since ω_1 and ω_2 copropagate and the blue light ω_4 should be produced in the forward direction. However, we did not try to observe

the presence of blue photons in the backward direction due to constraints in the experimental setup. The blue photons couple into the nanofiber and propagate along it. The guided light is coupled out of the ONF and passed through a 420 nm (FWHM: 10 nm) filter before reaching the single-photon counter (SPCM). The filter serves to eliminate any residual excitation beams, or other 780 nm photons, coupled to the nanofiber from the atom cloud or the MOT beams. Detection of blue photons serves as a signature of the two-photon absorption process in the evanescent field region; hence the ONF acts as both the excitation and detection tool simultaneously.

To study the influence of coupling and probe power on the two-photon process, we start with no ω_1 light through port A of the 50:50 splitter (Fig. 2). ω_2 is sent through port B and we observe blue emission from the cold-atom cloud. Hence, we deduce that excitation from $|1\rangle$ to $|2\rangle$ purely from the MOT beams is sufficient to initiate the two-photon process, which we observe for as little as 200 pW of power in ω_2. Figure 4(a) shows the typical blue counts detected on the SPCM when ω_2 was scanned across the two-photon transition. The peak in the observed spectrum occurs at the same two-photon frequency detuning as that which gives rise to the strongest observed transition in the vapor cell. When we plot the peak blue-photon count rate as a function of probe power in ω_2, we see there is saturation behavior even though we operate in the nW region [Fig. 4(b)].

The linewidth obtained for the two-photon spectrum from cold atoms [see Fig. 4(a)] is broader than the natural linewidths of the intermediate (∼5.9 MHz) and the final state (∼0.66 MHz) levels. This could arise from dephasing introduced to both of the levels due to the presence of MOT beams and the magnetic fields at all times during measurements. Power broadening and the ac Stark effect from the MOT beams would also give partial broadening. The other contributions in the broadening may come from the presence of the $5D_{5/2}$ state manifold and atom-fiber surface interactions [25,26]. Note that there is not much observable broadening when we only use a 780 nm probe beam for standard one-photon absorption (Fig. 3). This may be due to the effect of light-induced dipole forces on the atomic cloud [27]. In our case, we measure ∼14 MHz linewidth even when using nW of power.

Next, in order to study the effect of the very strong evanescent field intensities on atomic transitions, we introduce the coupling laser ω_1 into the ONF via port A of the fiber coupler. The power in the coupling beam, P_{ω_1}, is varied, while the probe power P_{ω_2} is fixed at 500 pW. This value was chosen to ensure that sufficient 420 nm photons are obtained for detection. We observe that the peak blue-photon count increases with P_{ω_1} and the width of the spectrum broadens (data not shown here). For $P_{\omega_1} \sim 20$ nW, the obtained spectrum clearly splits into two peaks. The peak separation increases as P_{ω_1} increases (Fig. 5). This is known as Autler-Townes (A-T) splitting and is caused by the ac Stark effect on the 780 nm transition in the presence of a strong-coupling beam [15]. The A-T splitting is plotted for different values of P_{ω_1} (see Fig. 6) and we see that it is directly proportional to the square root of P_{ω_1} as expected.

The number of blue photons detected via the optical nanofiber due to decay of the $6P_{3/2}$ level is related to the absorption of ω_2 light by the atoms. Therefore, considering a

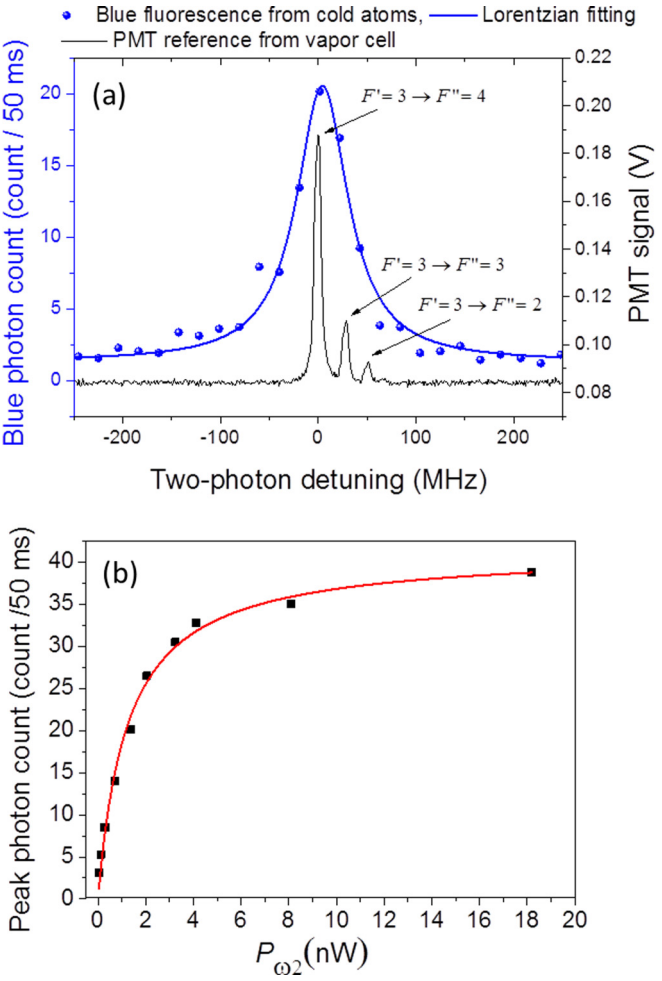

FIG. 4. (Color online) (a) 420 nm photon count rate (blue dots) as ω_2 is scanned across the $5P_{3/2}$ to $5D_{5/2}$ transition. An intermediate power (1.4 nW) of ω_2 is input into the nanofiber, whereas any 780 nm present is only from the MOT beams. The data are fitted (solid blue curve) to a Lorentzian profile. The black spectrum is the corresponding reference signal obtained from the vapor cell when the 780 and 776 nm beams are counterpropagating. The hyperfine transitions associated with each peak are indicated. (b) Maximum blue-photon count [i.e., the peak value of the curve in (a)] for different powers of ω_2. Here, the 780 nm contribution is also only from the MOT beams. The red curve is a theoretical fit to yield the saturation power as 1.24 ± 0.12 nW. This corresponds to ∼1.1 nW of 776 nm power at the waist.

simple three-level model, the observed A-T splitting spectrum is assumed to be proportional to the imaginary part of the density matrix term ρ_{32} [28],

$$\rho_{32} \propto \frac{i\frac{|\Omega_c^2|}{4}}{\gamma_{12}^2 + \delta_c^2 + 2\frac{|\Omega_c^2|}{4}} \frac{\gamma_{23} + i\delta_p}{[\gamma_{13} + i(\delta_p + \delta_c)][\gamma_{23} + i\delta_p] + \frac{|\Omega_c^2|}{4}}, \quad (1)$$

where γ_{12}, γ_{13}, and γ_{23} are dephasings, δ_c and δ_p are coupling and probe detunings, and Ω_c is the Rabi frequency of the coupling transition.

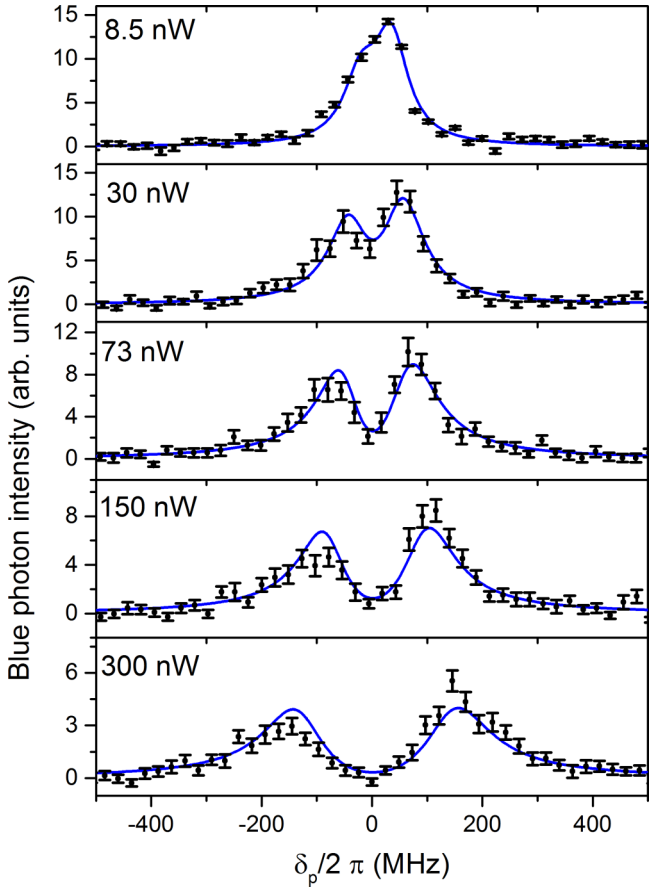

FIG. 5. (Color online) Blue fluorescence from the atoms collected via the ONF for different powers in ω_1, which is 14 MHz red detuned from the $5S_{1/2}$ $F = 2$ to $5P_{3/2}$ $F' = 3$ transition, while ω_2 is scanned across the $5P_{3/2}$ $F' = 3$ to $5D_{5/2}$ hyperfine levels. The power for ω_2 is fixed at 0.5 nW. δ_p is the detuning of ω_2 as indicated in Fig. 1. ω_1 is held at the same frequency as the cooling beams. Asymmetry in the observed A-T doublet is due to the fact that ω_1 is not on resonance. Solid lines are theoretical fits to the data using Eq. (1).

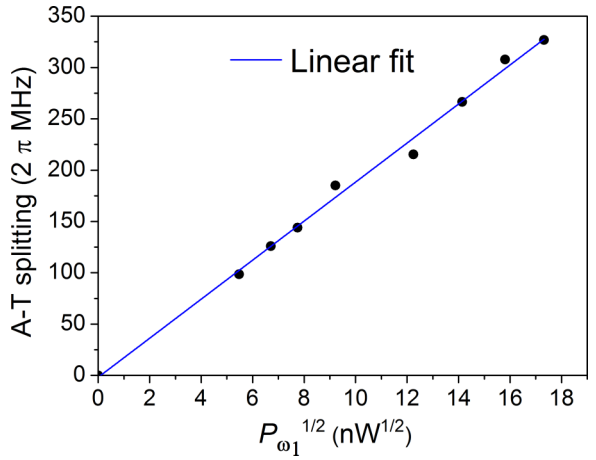

FIG. 6. (Color online) Measured A-T splitting as a function of the square root of the power in the 780 nm coupling beam.

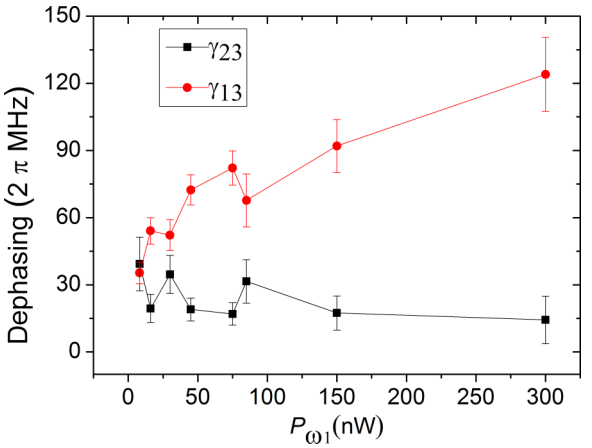

FIG. 7. (Color online) Variation of γ_{23} and γ_{13} as a function of coupling power P_{ω_1}.

Fitting Eq. (1) to the experimental data (Fig. 5), we obtain values for the dephasings and the Rabi frequency of the coupling transition. From the simplified model used, we find that γ_{13} is larger than γ_{23} and it increases with P_{ω_1} (Fig. 7). This behavior may be explained by the fact that the atom is a multilevel system and that very intense light fields are present; at higher P_{ω_1}, there is a finite probability that atoms may be excited from $5S_{1/2}$ $F = 2 \rightarrow 5P_{3/2}$ $F' = 2, 1$, thereby providing a decay channel for $5S_{1/2}$ $F = 2$, i.e., the lower hyperfine state, $5S_{1/2}$ $F = 1$. This mechanism may contribute to dephasing of the ground state and this is reflected by the increasing value of γ_{13} for higher P_{ω_1}. In order to gain better insight into the exact origin of the dephasings, a full theoretical description of a four-level system in the presence of an evanescent field is required. For a given power, the evanescent field distribution outside the nanofiber, the excitation probabilities, and the coupling efficiency of the 420 nm photons from atoms positioned at different radial distances from the ONF surface are needed. Heating of the atom cloud due to the excitation beams is also expected to play a role. As the power of ω_1 is increased, local temperature of the atom cloud should increase, thereby leading to a change in atom-cloud density and a possible increase in atom-atom or atom-surface interactions.

IV. CONCLUSION

We have observed frequency up-conversion and A-T splitting for ultralow-power levels (nW) in an atom-nanofiber system. The splitting is observed for ultralow powers of the coupling field in the evanescent region of the nanofiber. If we consider 50 nW of coupling power propagating in the ONF, we can assume that there is typically less than one photon in the interaction volume at any given time [12,29]. Such power levels are used frequently in nanofiber experiments and it is important to take into account any induced shifts in the energy levels that may arise [30]. In the high-intensity regime, the Rabi frequency for the coupling transition is approximately equal to the A-T splitting [31] and this method allows us to measure it directly for an atom+nanofiber system. Otherwise, due to the difficulties in exactly determining nanofiber parameters, such as the influence of fiber surface on energy levels, the

effective position of the atoms in the evanescent field, the waist size of the ONF, etc., this could be challenging to estimate. The observation of nonlinear phenomena using an ONF in a cold-atom system increases the versatility of such devices and may be useful for demonstrations of single-photon all-optical switching [32], or quantum logic gates [33] at ultralow powers. The efficiency of the process may be improved by optimizing the beam polarizations [34] at the nanofiber waist, a technique that relies on optimum control of light propagation in ultrathin fibers [19,35,36].

ACKNOWLEDGMENTS

This work was supported by the Okinawa Institute of Science and Technology Graduate University. S.N.C. is grateful to JSPS for partial support from a Grant-in-Aid for Scientific Research (Grant No. 26400422). The authors would like to thank H. Ritsch, E. Brion, M. Lepers, R. Guérot, and Y. Zhang for useful discussions.

R.K. and V.G. contributed equally to this work.

[1] K. P. Nayak, P. N. Melentiev, M. Morinaga, F. L. Kien, V. I. Balykin, and K. Hakuta, Opt. Express **15**, 5431 (2007).

[2] M. J. Morrissey, K. Deasy, Y. Wu, S. Chakrabarti, and S. Nic Chormaic, Rev. Sci. Instrum. **80**, 053102 (2009).

[3] L. Russell, K. Deasy, M. J. Daly, M. J. Morrissey, and S. Nic Chormaic, Meas. Sci. Tech. **23**, 015201 (2012).

[4] E. Vetsch, D. Reitz, G. Sagué, R. Schmidt, S. T. Dawkins, and A. Rauschenbeutel, Phys. Rev. Lett. **104**, 203603 (2010).

[5] A. Goban, K. S. Choi, D. J. Alton, D. Ding, C. Lacroûte, M. Pototschnig, T. Thiele, N. P. Stern, and H. J. Kimble, Phys. Rev. Lett. **109**, 033603 (2012).

[6] J. E. Hoffman, J. A. Grover, Z. Kim, A. K. Wood, J. R. Anderson, A. J. Dragt, M. Hafezi, C. J. Lobb, L. A. Orozco, S. L. Rolston, J. M. Taylor, C. P. Vlahacos, and F. C. Wellstood, Rev. Mex. Fís. **57**, 1 (2011), arXiv:1108.4153.

[7] J.-B. Béguin, E. M. Bookjans, S. L. Christensen, H. L. Sørensen, J. H. Müller, E. S. Polzik, and J. Appel, Phys. Rev. Lett. **113**, 263603 (2014).

[8] M. Fleischhauer, A. Imamoglu, and J. P. Marangos, Rev. Mod. Phys. **77**, 633 (2005).

[9] A. K. Patnaik, J. Q. Liang, and K. Hakuta, Phys. Rev. A **66**, 063808 (2002).

[10] L. Russell, M. Daly, and S. Nic Chormaic, AIP Conf. Proc. **1469**, 82 (2012).

[11] S. M. Spillane, G. S. Pati, K. Salit, M. Hall, P. Kumar, R. G. Beausoleil, and M. S. Shahriar, Phys. Rev. Lett. **100**, 233602 (2008).

[12] S. M. Hendrickson, M. M. Lai, T. B. Pittman, and J. D. Franson, Phys. Rev. Lett. **105**, 173602 (2010).

[13] T. B. Pittman, D. E. Jones, and J. D. Franson, Phys. Rev. A **88**, 053804 (2013).

[14] R. E. Ryan, L. A. Westling, and H. J. Metcalf, J. Opt. Soc. Am. B **10**, 1643 (1993).

[15] S. H. Autler and C. H. Townes, Phys. Rev. **100**, 703 (1955).

[16] R. W. Fox, S. L. Gilbert, L. Hollberg, J. H. Marquardt, and H. G. Robinson, Opt. Lett. **18**, 1456 (1993).

[17] M. J. Piotrowicz, C. MacCormick, A. Kowalczyk, S. Bergamini, I. I. Beterov, and E. A. Yakshina, New J. Phys. **13**, 093012 (2011).

[18] H. Zhang, L. Wang, J. Chen, S. Bao, L. Zhang, J. Zhao, and S. Jia, Phys. Rev. A **87**, 033835 (2013).

[19] R. Kumar, V. Gokhroo, K. Deasy, A. Maimaiti, M. C. Frawley, C. Phelan and S. Nic Chormaic, New J. Phys. **17**, 013026 (2015).

[20] J. E. Bjorkholm and P. F. Liao, Phys. Rev. A **14**, 751 (1976).

[21] J. M. Ward, A. Maimaiti, Vu H. Le, and S. Nic Chormaic, Rev. Sci. Instrum. **85**, 111501 (2014).

[22] M. B. Kienlen, N. T. Holte, H. A. Dassonville, A. M. C. Dawes, K. D. Iversen, R. M. McLaughlin, and S. K. Mayer, Am. J. Phys. **81**, 442 (2013).

[23] O. S. Heavens, J. Opt. Soc. Am. **51**, 1058 (1961).

[24] A. M. Akulshin, R. J. McLean, A. I. Sidorov, and P. Hannaford, Opt. Express **17**, 22861 (2009).

[25] F. Le Kien and K. Hakuta, Phys. Rev. A **75**, 013423 (2007).

[26] V. G. Minogin and S. Nic Chormaic, Laser Phys. **20**, 32 (2009).

[27] G. Sagué, E. Vetsch, W. Alt, D. Meschede, and A. Rauschenbeutel, Phys. Rev. Lett. **99**, 163602 (2007).

[28] T. Y. Abi-Salloum, J. Mod. Opt. **57**, 1366 (2010).

[29] L. Tong, J. Lou, and E. Mazur, Opt. Express **12**, 1025 (2004).

[30] J. Lee, J. A. Grover, J. E. Hoffman, L. A. Orozco, and S. L. Rolston, arXiv:1412.6754.

[31] S. Stenholm, *Foundations of Laser Spectroscopy* (Wiley, New York, 1984).

[32] S. M. Hendrickson, C. N. Weiler, R. M. Camacho, P. T. Rakich, A. I. Young, M. J. Shaw, T. B. Pittman, J. D. Franson, and B. C. Jacobs, Phys. Rev. A **87**, 023808 (2013).

[33] S. Krishnamurthy, Y. Wang, Y. Tu, S. Tseng, and M. S. Shahriar, Opt. Express **21**, 24514 (2013).

[34] A. Vernier, S. Franke-Arnold, E. Riis, and A. S. Arnold, Opt. Express **18**, 17020 (2010).

[35] S. Ravets, J. E. Hoffman, P. R. Kordell, J. D. Wong-Campos, S. L. Rolston, and L. A. Orozco, J. Opt. Soc. Am. A **30**, 2361 (2013).

[36] R. Mitsch, C. Sayrin, B. Albrecht, P. Schneeweiss, and A. Rauschenbeutel, Phys. Rev. A **89**, 063829 (2014).